Investigating the influence of different thermodynamic paths on the structural relaxation in a glass-forming polymer melt

1999 J. Phys.: Condens. Matter 11 2179

(http://iopscience.iop.org/0953-8984/11/10/005)

J. Phys.: Condens. Matter **11** (1999) 2179–2192. Printed in the UK PII: S0953-8984(99)97794-9

Investigating the influence of different thermodynamic paths on the structural relaxation in a glass-forming polymer melt

Christoph Bennemann, Wolfgang Paul, Jörg Baschnagel and Kurt Binder
Institut für Physik, 55099 Mainz, Germany

Received 23 September 1998, in final form 14 January 1999

Abstract. We present results from molecular dynamics simulations of the thermal glass transition in a dense polymer melt. In previous work we compared the simulation data with the idealized version of mode-coupling theory (MCT) and found that the theory provides a good description of the dynamics above the dynamical critical temperature. In order to investigate the influence of different thermodynamic paths on the structural relaxation (α-process), we performed simulations for three different pressures and are thus able to give a sketch of the critical line of MCT in the pressure–temperature plane, where, according to the idealized version of MCT, an ergodic–nonergodic transition should occur. Furthermore, by cooling our system along two different paths (an isobar and an isochor), with the same intersection point of the critical line, we demonstrate that neither the dynamical critical temperature nor the exponent γ depend on which path is chosen.

1. Introduction

The understanding of the glass transition has been a long-standing problem of condensed matter physics and materials science [1–4]. The term *glass transition* is used to describe a phenomenon where a solidification of a liquid without simultaneous crystallization occurs. In a narrow temperature region, the viscosity of the material increases by some 14 orders of magnitude, while no significant change in the structure is observed and the material remains amorphous.

Experimental research in this field has been conducted for more than a hundred years [1,5]. Since then a large number of phenomenological theories have been proposed, such as the free-volume theory [6–8] and the Gibbs–Di Marzio theory [9–12], to explain the characteristic features of the glass transition. These theories mainly deal with thermodynamic properties and the Vogel–Fulcher law [1] for the temperature dependence of the viscosity, i.e., with the behaviour at low temperatures close to the temperature of seeming divergence of the viscosity. However, an explicit relationship between the model parameters and the microscopic properties of the glass former remained hard to establish, and a detailed description of the shape of the dynamic correlation functions was not attempted.

In recent years, mode-coupling theory (MCT) was successful in describing a broad range of features observed in experiments [13–17] and simulations [18–26] (also see [27] for an overview) in a temperature region close to a so-called dynamical critical temperature T_c, which in general lies above the empirically defined glass transition temperature T_g. This dynamical critical temperature is approximately equal to the temperature of the strong bend in the graph of viscosity against temperature for fragile liquids and is associated with a change in dynamics from a liquid-like to a solid-like behaviour. This theory starts from well known microscopic

0953-8984/99/102179+14$19.50

dynamics and uses techniques already applied in the field of critical dynamics to derive a set of dynamic equations for the density correlation functions of the system [28–31] (also see [32,33] for review articles). In real systems, with the probable exception of some colloidal glasses [14], activated processes neglected in the idealized version of the theory restore the ergodicity below T_c also.

Although MCT has been applied to experimental data numerous times, many aspects of the theory still remain to be thoroughly investigated. Little is known on the influence of external thermodynamic parameters on the transition temperature (although see [34–37]) or the α-process. Since in general higher pressure causes higher densities, which in turn means that the movement of an individual particle is more hindered, an increase in pressure results in an increase of the glass transition temperature [4]. Hence, it is possible to cause a glass transition solely by increasing the pressure, which indeed has been observed in experiment [37].

In general the thermodynamic parameter space (for instance, the (p, T) plane) should decompose into two areas, a fluid phase and an ideal-glass phase, separated by a critical line at which the transition to nonergodicity should occur. Since MCT applies to systems in thermodynamic equilibrium, the position of the critical line should be independent of the thermodynamic path chosen for the cooling. Furthermore, close to the critical line, the exponents of the theory, which determine most of the quantitative behaviour of the glass former, depend solely on the intersection point of the thermodynamic path with the critical line, provided that one does not choose too exotic a path, e.g. one that runs almost parallel to the critical line. Therefore two different thermodynamic paths, which have the same intersection point with the critical line, should not only yield the same critical temperature, but also the quantitative behaviour of the systems, described in terms of MCT, should be the same along both of them. To our knowledge, so far this prediction has never been verified.

Thus, we decided to study the influence of pressure on the parameters of the ideal MCT. To this end, we chose a model for a glass-forming polymer melt which has been used previously [26]. Clearly, because of the connectivity of the monomers along the chain, our model is by no means a simple liquid, and therefore certainly not the kind of system for which ideal MCT was originally developed. On the other hand, polymers, according to Angell's classification scheme [38], mostly belong to the group of fragile glass formers, to which MCT has been applied successfully, and are extremely good glass formers, i.e. 'supercooled' melts in thermal equilibrium can be prepared very well. In previous work [26] it was demonstrated that it is possible to equilibrate our model well in the regime of the supercooled melt, a prerequisite for applying MCT, and that the α-relaxation behaviour is compatible with MCT. By simulating the system in the isochoric (NVT-) as well as in the isobaric (NpT-) ensemble, we try to test the prediction of thermodynamic path independence in the present paper. To this end, we cooled our system along an isochoric path which shared its intersection point with the critical line with one of the isobaric paths. As in our earlier work [26], we concentrate on the α-relaxation behaviour in this study. An analysis of the β-relaxation can be found in reference [39].

The remainder of the paper is organized as follows. In section 2 we briefly describe our model and the simulation technique. By performing simulations along different isobars we were able to investigate the influence of pressure on the dynamical critical temperature. The results of these simulations will be discussed in section 3. In section 4 we will perform a test of the thermodynamic path independence and in section 5 conclusions will be drawn.

2. The model and simulation technique

For modelling the inter- and intramolecular forces we used a bead–spring model derived from the one suggested by Kremer and Grest [40] and also used in several recent simulations [41,42].

However, here we included also the attractive part of the Lennard-Jones potential, since previous work on a lattice model for a glassy polymer melt [43, 44] had shown that without such an attraction a negative thermal expansion coefficient would result. The model of Kremer and co-workers [40–42] is close to an athermal model of polymer melts and hence does not exhibit a glass transition driven by temperature at all.

As in our past simulations, each chain consisted of ten beads with mass m set to unity. Although these chains are rather short, they already show the static behaviour characteristic of long polymers in the melt (e.g. Gaussian statistics for the end-to-end-distance distribution, a Debye scattering law for the single-chain structure factor, etc). Note that each bond in this model would correspond to $n \approx 3$–6 covalent bonds along the backbone of a real chain, if one were to map this coarse-grained model onto a real polymer. Between all monomers there acted a truncated Lennard-Jones potential:

$$U_{\mathrm{LJ}}(r_{ij}) = \begin{cases} 4\epsilon\left[\left(\dfrac{\sigma}{r_{ij}}\right)^{12} - \left(\dfrac{\sigma}{r_{ij}}\right)^{6}\right] + C & r_{ij} < 2\cdot 2^{1/6}\sigma \\ 0 & r_{ij} \geqslant 2\cdot 2^{1/6}\sigma \end{cases} \tag{1}$$

where C was a constant which guaranteed that the potential was continuous everywhere. Since it was not our aim to simulate a specific polymer, we used Lennard-Jones units, where ϵ and σ are set to unity. Note that this means that all quantities are dimensionless. In addition to the Lennard-Jones potential, a FENE backbone potential was applied along the chain:

$$U_{\mathrm{F}}(r_{ij}) = -\frac{k}{2}R_0^2 \ln\left[1 - \left(\frac{r_{ij}}{R_0}\right)^2\right]. \tag{2}$$

The parameters of the potential were taken as $k = 30$ and $R_0 = 1.5$, guaranteeing a certain stiffness of the bonds while avoiding high-frequency modes and chain crossing. Furthermore, with these parameters we set the favoured bond length to a value slightly smaller than the length favoured by the Lennard-Jones potential. Thus we introduced two different incompatible length scales in our system, which prevents the emergence of long-range order (i.e. crystal formation) at lower temperatures.

Unlike previous lattice models for the thermally driven glass transition of polymers [43, 44], the present model has a qualitatively reasonable equation of state with a positive thermal expansion coefficient, and can easily be studied at constant density or constant pressure. It allows us to study motion and structure from local scales (motions in the neighbour cage) up to large scales.

In order to keep the temperature fixed, all simulations were performed using a Nosé–Hoover thermostat [45–47]. In this technique the model system is coupled to a heat bath, which represents an additional degree of freedom. To set the system to a desired pressure, the size of the simulation box was adjusted to yield the correct density at each temperature. The resulting configurations were used as start configurations for runs in the canonical ensemble, where the size of the simulation box was kept fixed. Only during these canonical runs were dynamic correlation functions for use in further analysis calculated. A more thorough discussion of the simulation technique applied can be found elsewhere [26, 48]. Here we only emphasize that we have carefully checked that the Nosé–Hoover thermostat does not lead to any artefacts in the dynamics of the single-chain correlators and local properties that were studied here [48]. Note also that our chain length $N = 10$ was short enough that our results are not affected at all by chain entanglement effects.

Altogether, we performed simulations at more than 40 different points in the thermodynamic phase space. At each point, ten independent configurations were simulated, each consisting of 120 polymer chains of ten monomers. In this way, we were able to perform

Table 1. The table shows at which temperatures and densities or pressures the simulations were performed.

Ensemble	Simulation temperatures
Isochor ($\rho = 1.042$)	0.5, 0.52, 0.55, 0.58, 0.6, 0.65, 0.7, 0.8, 0.9, 1.0, 2.0
Isobar ($p = 0.5$)	0.45, 0.48, 0.5, 0.52, 0.55, 0.6, 0.7, 1.0
Isobar ($p = 1.0$)	0.46, 0.47, 0.48, 0.49, 0.5, 0.52, 0.55, 0.6, 0.65, 0.7, 1.0, 2.0, 4.0
Isobar ($p = 2.0$)	0.52, 0.55, 0.57, 0.6, 0.7, 0.8, 0.9, 1.0, 2.0

simulations along three isobars and one isochor. Table 1 shows for which temperatures simulations were made and in which ensemble.

In order to equilibrate an individual system at lower temperatures, one had to simulate for very long times ($>10^6$ MD steps). Generally, the equilibration of the lowest temperature in a given ensemble lasted as long as the sum of all equilibration times at higher temperatures for the same ensemble. Altogether, the simulations consumed an equivalent of approximately 10 CPU years on a Pentium Pro® processor run at 180 MHz.

3. Dynamical properties at different pressures

As already discussed in the opening paragraph, the glass transition manifests itself by a steep increase of the relaxation times. In order to extract these timescales from the simulation data, we computed a number of dynamical quantities, like the incoherent intermediate dynamic structure factor:

$$\phi_q^s(t) = \left\langle \frac{1}{M} \sum_{i=1}^{M} e^{i\boldsymbol{q}\cdot(\boldsymbol{r}_i(t)-\boldsymbol{r}_i(0))} \right\rangle \tag{3}$$

where M stands for the total number of monomers in the melt. This function measures the self-correlation of the particle positions at different times and, on varying the wave-vector $\boldsymbol{q}$, at different length scales.

Recently, orientational degrees of freedom and their relaxational behaviour have become a focus of theoretical research on the glass transition [49, 50]. Results of molecular dynamics simulations for a fluid consisting of diatomic molecules [22–24] illustrated that there can be significant differences between orientational and translational relaxation. Such differences are also observed in experiments (see reference [55], for instance). Clearly, it should be interesting to check whether we could find any differences between orientational and translational relaxation in our model. Hence, we also calculated the orientational correlation of the end-to-end vector:

$$E_n(t) \equiv \left\langle L_n\left(\frac{\boldsymbol{e}(t)\cdot\boldsymbol{e}(0)}{||\boldsymbol{e}(t)||\,||\boldsymbol{e}(0)||} \right) \right\rangle \qquad n = 1, 2, \ldots \tag{4}$$

where L_n stands for the nth Legendre polynomial, $\boldsymbol{e}(t)$ is the end-to-end vector of a polymer at time t and $||\boldsymbol{e}||$ is the length of the end-to-end vector at time t. The same formula can be applied to measure the dynamical correlation of a bond vector $\boldsymbol{b}(t)$:

$$B_n(t) \equiv \left\langle L_n\left(\frac{\boldsymbol{b}(t)\cdot\boldsymbol{b}(0)}{||\boldsymbol{b}(t)||\,||\boldsymbol{b}(0)||} \right) \right\rangle \qquad n = 1, 2, \ldots. \tag{5}$$

Equations (4) and (5) characterize the reorientation dynamics of the largest and of the smallest vectors along the backbone of a chain. In the analysis, we only calculated the first and second polynomial, since these quantities can be measured by dielectric relaxation and light scattering, respectively.

With these three dynamical correlation functions we define the following correlation times:

$$\phi_q^s(\tau_q) = 0.3 \qquad E_n(\tau_{E_n}) = 0.3 \qquad B_n(\tau_{B_n}) = 0.3. \tag{6}$$

The value of 0.3 is chosen for convenience and our conclusions do not depend on a variation of this value within a reasonable range (1/e, 0.5). We have computed a number of other related quantities as well, such as the Rouse modes of the system and the mean square displacements, which are discussed in other publications [26, 39, 56].

3.1. The behaviour of dynamical correlators

As shown in figure 1 and figure 2, the correlators decay in one step at high temperatures, while at lower temperatures a two-step process starts to emerge, which becomes more pronounced as the temperature becomes lower. The emergence of a plateau in the decay is related to the cage effect [29], where an individual monomer is trapped by its surrounding particles. The average time that a monomer needs to escape from the cage of its neighbours increases with decreasing temperature, which explains the extension of the plateau. The presence of a two-step relaxation, the so-called β-relaxation (onto and off the plateau) and α-relaxation (off the plateau and long-time structural relaxation), is a common feature of glass formers, and is also predicted by MCT.

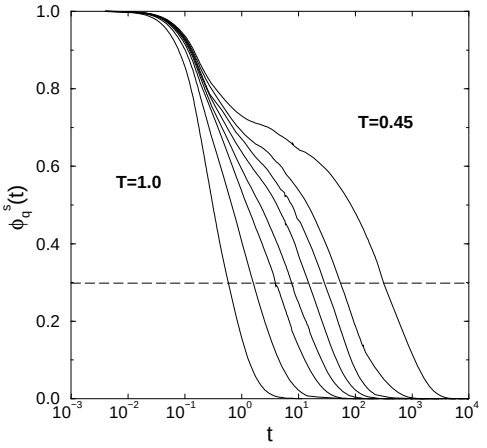

Figure 1. Intermediate dynamic structure factors at the first maximum of the static structure factor ($q = 6.9$) [39] measured along the isobar $p = 0.5$. The broken line shows the value which we used to define the α-relaxation timescale. From left to right the temperatures decrease, as specified in table 1.

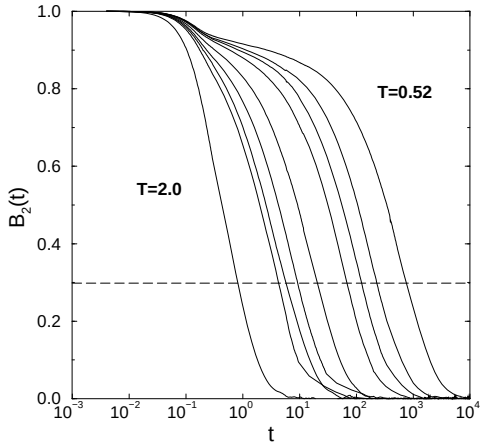

Figure 2. Dynamic correlation functions of the orientation of the bond vectors (the second Legendre polynomial; see equation (5)) for $p = 2.0$. From left to right the temperatures decrease, as specified in table 1.

The qualitative behaviour is not affected by the applied pressure (we therefore only show the behaviour for $p = 0.5$ in figure 1), although at higher pressure the two-step process already starts to appear at higher temperatures. Furthermore, while the height of the plateau depends on the specific correlator, it hardly varies with pressure. The orientational correlators (first and second Legendre polynomials; see equations (4) and (5)) exhibit a rather high plateau value which is often close to unity (the plateau of the first Legendre polynomial is always larger than that of the second). Therefore the two-step process is only visible on magnification. Clearly, the contribution of the α-process to the overall relaxation of a correlator depends on the quantity considered.

Another characteristic of glass-forming liquids is that close to the dynamical critical temperature the time–temperature superposition principle should hold for the α-relaxation. One therefore has to rescale a dynamical correlator with respect to a suitably defined α-relaxation time and to check whether the curves fall on a master curve in the α-regime. As we reported in our earlier work for $p = 1$ (and constant volume) [26], this is indeed the case. Here, we additionally observe that our data also obey a time–temperature–pressure superposition principle, i.e., in the α-regime, data taken from different isobars collapse onto a single master curve. This is illustrated for the incoherent scattering function and the second Legendre polynomial of the bond-vector autocorrelation function in figure 3, where fourteen different curves are included in one plot. The fact, that we observe this time–temperature–pressure scaling also means that the stretching exponent in the Kohlrausch–Williams–Watts law, which one can fit to the α-decay, would not depend on pressure in the range of pressures that we studied. Similar behaviour has been observed in experiments on orthoterphenyl [36], but, to the best of our knowledge, this is the first report from computer simulations for such a behaviour.

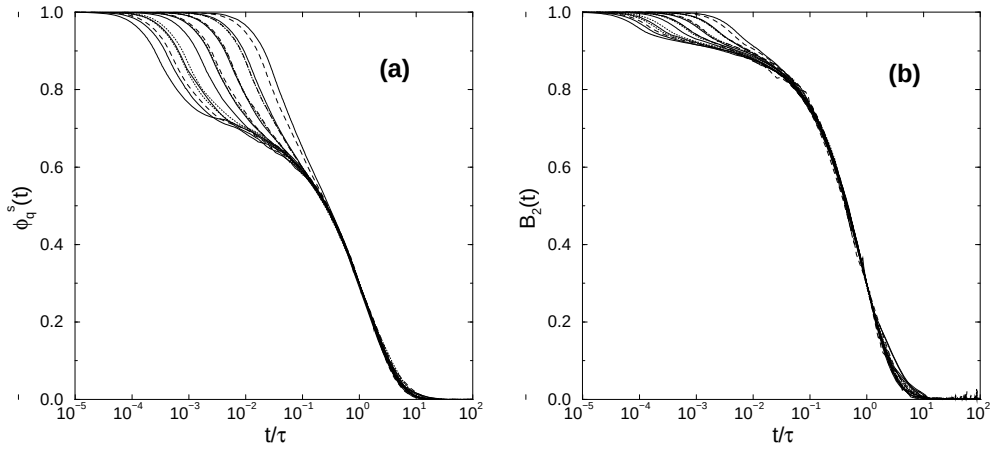

Figure 3. Panel (a) is a compilation of the results for the intermediate-scattering function, but with times scaled with respect to the α-relaxation timescale for selected temperatures close to the critical temperature at the respective pressure: $T = 0.45, 0.48, 0.5, 0.52, 0.55$ for $p = 0.5$ (dashed curves), $T = 0.46, 0.47, 0.48, 0.5, 0.52$ for $p = 1$ (solid curves) and $T = 0.52, 0.55, 0.57, 0.6$ for $p = 2$ (dotted curves). In the α-regime the curves for different temperatures and pressures all collapse onto a single master curve, demonstrating time–temperature–pressure superposition. Panel (b) shows the same behaviour for the orientational correlation function $B_2(t)$ (the second Legendre polynomial) of the bonds.

3.2. The behaviour of the relaxation times

Figures 1 and 2 show that on lowering the temperature an increase of the relaxation times by several orders of magnitude takes place, as expected for a glass-forming liquid. The idealized MCT predicts that sufficiently close to T_c the increase of the α-relaxation times can be described by the following formula:

$$\tau = \tau^0 (T - T_c)^{-\gamma} \tag{7}$$

where τ^0 is an amplitude which depends on the specific relaxation time considered, and γ is a parameter of the theory which should be the same for all correlation times, if the corresponding

correlator couples to density fluctuations. Furthermore, our analysis of the β-regime suggested that γ should take the value of $\gamma = 2.09$ for the isobar $p = 1.0$ [39].

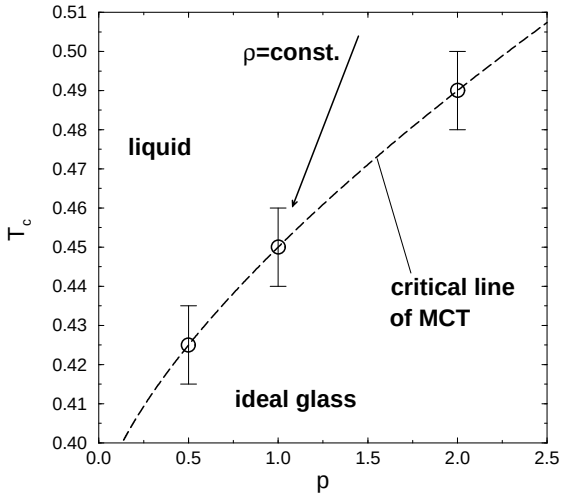

Figure 4. Mode-coupling critical temperatures at different pressures. The critical temperatures represent averages which are derived by fitting equation (7) to all relaxation times shown in figure 5. The broken curve is an illustration of the critical line of MCT (a guide to the eye only), while the arrow symbolizes a thermodynamic path at constant density.

Table 2. Critical temperatures and densities, and the soft-sphere scaling variable at the critical point.

p	T_c	ρ_c	$\rho_c T_c^{-1/4}$
0.5	0.425 ± 0.010	1.035 ± 0.01	1.28 ± 0.02
1.0	0.450 ± 0.005	1.042 ± 0.01	1.27 ± 0.02
2.0	0.490 ± 0.010	1.054 ± 0.01	1.26 ± 0.02

At all pressures investigated, it is indeed possible to locate a temperature interval where the increase of the relaxation times can be described by equation (7). When applying equation (7), τ^0, T_c and γ were treated as adjustable parameters. Although it is not incompatible with MCT for rotational and translational degrees of freedom to freeze at different state points in the temperature–density plane, as was demonstrated in recent publications [49, 50], our analysis suggests that it is possible to find a dynamical critical temperature for all isobaric paths which is independent of the specific correlator and solely a function of the pressure considered. The critical temperatures and densities obtained are listed in table 2. Note that the error for the critical temperature for $p = 1.0$ is smaller than for the other pressures because simulations for a larger number of temperatures were carried out for this isobar. The pressure dependence of the dynamical critical temperature is depicted in figure 4. As expected, the critical temperature increases with increasing pressure as was also calculated for Lennard-Jones models in [34]. As one can also see from table 2, within the error bars the quantity $\rho_c T_c^{-1/4}$ is a constant at the mode-coupling critical point, as was also found experimentally in e.g. [37] and in the simulation of soft-sphere models [51–53] and for Lennard-Jones mixtures [54]. The value that we found is, within the error bars, identical to the Lennard-Jones value given in [54].

Figure 5 shows a double-logarithmic plot of α-relaxation times against $T - T_c$, using the critical temperatures of equation (2). For all pressures there is a temperature interval where the data points lie on a straight line in accord with equation (7). Deviations from the power-law behaviour are visible both at small and large distances from the critical point. The deviations

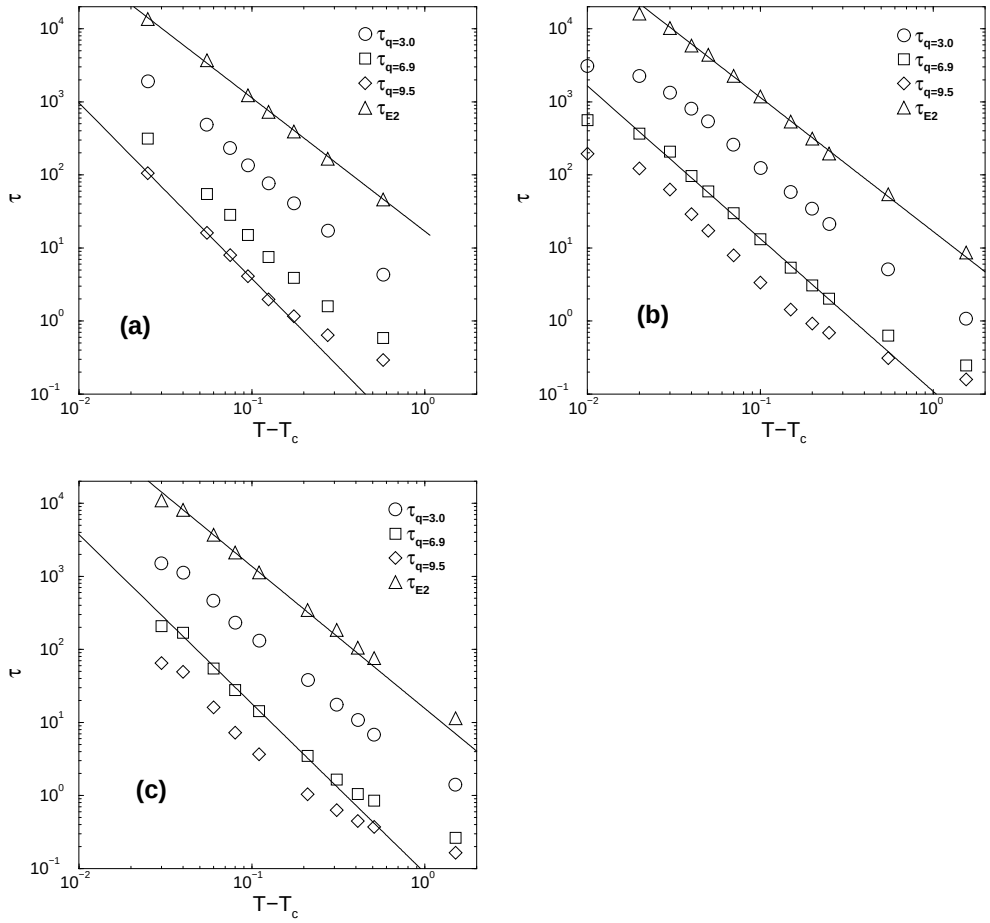

Figure 5. The temperature behaviour of different relaxation times, measured along the isobars $p = 0.5$ (a), $p = 1.0$ (b) and $p = 2.0$ (c). In the plots, τ_q and τ_{E_2} are the α-relaxation times of the incoherent dynamic structure factor at different wavenumbers and the dynamic orientational correlation of the end-to-end vector (second Legendre polynomial), respectively. The values of T_c are listed in table 2. The solid lines are power-law fits, including the largest possible number of temperatures. For $p = 1$, the fit for $q = 6.9$ uses $\gamma = 2.09$, i.e., the γ-value resulting from an analysis of the β-relaxation [39].

for large $T - T_c$ are expected because equation (7) is an asymptotic expansion which is only valid if the reduced distance to T_c, i.e., $(T - T_c)/T_c$, is small. The upper bounds for the validity of equation (7) are approximately 0.7 ($p = 0.5$), 1.2 ($p = 1$) and 0.6 ($p = 2$), which are comparable to the results from experiments [13, 15] and other simulations [20–24]. However, these upper bounds strongly depend on the quantity under consideration. Whereas deviations are very pronounced for the smallest length scale ($q = 9.5$), equation (7) provides a good description at all except perhaps the lowest temperatures for the end-to-end-distance orientational autocorrelation function.

On the other hand, the deviations from the idealized power law at low temperatures could be attributed to the ergodicity-restoring thermally activated processes mentioned above. Close to the dynamical critical temperature, these processes start to contribute significantly to the relaxation dynamics of the system, and therefore the actual relaxation times can be smaller than

the predictions of idealized MCT. This behaviour has been discussed in experimental studies, e.g. [13, 15], and simulation studies, e.g. [19, 22, 23]. Therefore, in practical applications of equation (7) one faces the problem that its range of validity is limited from below and above, and that it additionally depends on the quantity under consideration.

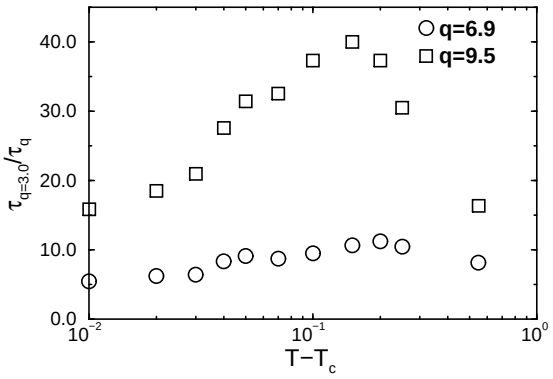

Figure 6. The ratio of different α-relaxation times as measured along the isobar $p = 1.0$. As can be seen, even close to the critical temperature ($T_c = 0.45$) the ratio changes by almost a factor of two.

Furthermore, equation (7) implies that in the temperature regime where the idealized MCT is applicable, the ratio of two different α-relaxation times should be independent of temperature. As demonstrated in figure 6, this is not the case, even in the regime where the β-analysis could be done, i.e., for $T - T_c \leqslant 0.07$ [39]. The ratio between different relaxation times can change by almost a factor of two, and the effect is stronger for $q = 9.5$ than for $q = 6.9$ (the first minimum and maximum of the static structure factor, respectively). Note that we obtain the same result when applying a different definition of the α-relaxation time which includes the nonergodicity parameter f_q^{sc}, i.e., $\phi_q^s(\tau_q) = e^{-1} f_q^{sc}$. However, it is not clear whether this finding is a strong contradiction to MCT, because we have eliminated the dominant temperature dependence, given by equation (7), when dividing two relaxation times. Since we are considering a temperature range that is close, but not very close, to T_c, and equation (7) is, strictly speaking, only asymptotically valid, one could expect a smooth temperature dependence of the prefactors. Such a conclusion can also be drawn from reference [16], in which the MCT equations for a model of a colloidal suspension are solved numerically and compared with the asymptotic results. There, it is found that the ratio of two relaxation times becomes constant only very close to the critical point, although equation (7) is already followed for larger distance to the critical volume fraction (see figure 7 of reference [16]). Interestingly, figure 6 shows that the ratio is not a monotonic function and exhibits a maximum approximately at the beginning of the temperature interval in which we can apply ideal MCT to describe the α-relaxation time. It seems as if at this temperature a change in the dynamics of the system occurs.

This problem is also reflected in figure 7 which shows the results for γ when fitting equation (7) to the α-relaxation time of $\phi_q^s(t)$ at $p = 1$. The critical temperature was kept fixed ($T_c = 0.45$) in the fits, and the maximum possible number of temperatures were taken into account to determine γ. It is interesting to note that the γ-values, determined from figure 5 for the different pressures, agree with one another within the error margins, so the following discussion is not specific to $p = 1$. Figure 7 shows that the fit procedure yields a decrease of γ with decreasing q, but the γ-values are distributed around the result of the β-relaxation analysis, $\gamma = 2.09$ [39]. Alternatively, one can keep the exponent $\gamma = 2.09$ constant and adjust the critical temperature, T_c [39]. Then the critical temperatures for $q \geqslant 3$ coincide, within the error bars, with the value obtained from the β-analysis. However, the diffusion

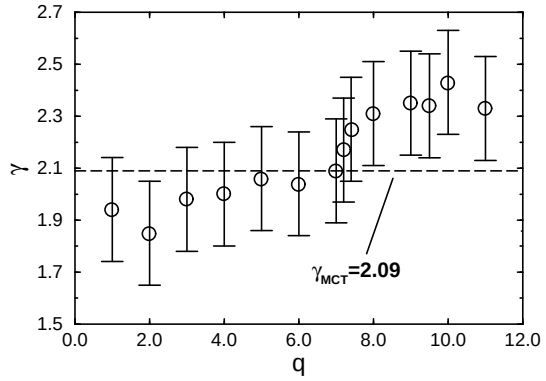

Figure 7. The variation of γ ($p = 1.0$) with the magnitude q of the wave-vector when fitting the α-relaxation time of $\phi_q^s(t)$ with equation (7) while keeping the critical temperature fixed ($T_c = 0.45$).

coefficient of a chain yields a value of T_c which is significantly lower. Physically, both types of analysis suggest that, going from T_c to higher temperatures, the melt has a stronger tendency to liquify on short than on the long length scales. Such a behaviour is not unique to our polymer model, but it was also found in other simulations [20, 22].

4. Testing of the thermodynamic path independence

In order to verify the prediction of thermodynamic path independence, we estimated the density of the melt at the critical temperature ($T_c = 0.45$) of the isobar $p = 1$. The density is $\rho = 1.042$. Then we performed a number of simulations in the NVT-ensemble for the appropriate isochor (schematically, this is illustrated in figure 4), and again calculated various dynamic correlation functions at the simulation temperatures (see table 1).

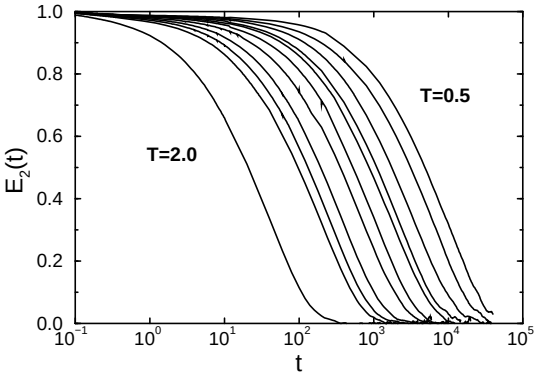

Figure 8. Dynamic correlation of the end-to-end-vector orientation (the second Legendre polynomial), as measured at constant density along the thermodynamic path $\rho = 1.042$. Temperature decreases from right to left, as specified in table 1.

The qualitative behaviour of the dynamical correlation functions along this isochor does not differ from the behaviour observed for the various isobars, discussed in the preceding section. As can be seen in figure 8 and figure 9, which show as an example the dynamic correlation of the end-to-end-vector orientation, we find again that at lower temperatures a two-step relaxation occurs (which cannot be seen on the scale of the figures due to the large plateau value), that the relaxation times show a steep increase and that, at least for the lower temperatures, the time–temperature superposition principle holds. This could have been expected, since earlier

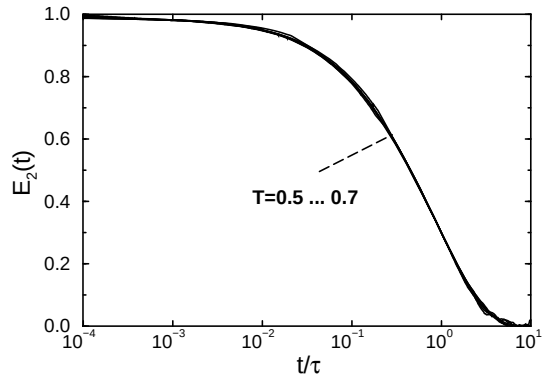

Figure 9. An α-scaling plot of the end-to-end-vector correlation function for temperatures ranging from $T = 0.5$ to $T = 0.7$ (see table 1 for details). The simulation data are for the same isochor as was shown in figure 8, and the relaxation time was determined by equation (6).

simulations of the model in the NVT-ensemble had also shown such a behaviour [26]. It is interesting to note, however, that, compared to the appropriate isobar, the two-step relaxation process can now be already observed at higher temperatures and that for the temperatures studied the α-relaxation time is almost one order of magnitude larger.

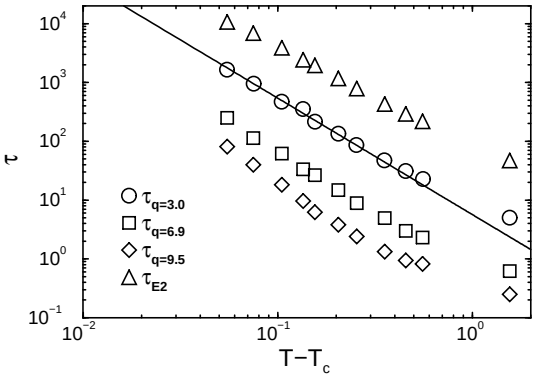

Figure 10. The temperature behaviour of different α-relaxation times, as measured in the NVT-ensemble. The solid line represents a fit with equation (7).

Once again it is possible to find a temperature region where the behaviour of the α-relaxation times, extracted from the different dynamic correlation functions, can be described by equation (7). This is illustrated in figure 10, where we show the temperature dependence of various correlation times, as measured in the NVT-ensemble, plotted in such a way that the applicability of the MCT prediction is clearly demonstrated. Qualitatively, we find the same features as discussed before for the isobars. There are deviations from linearity at large temperatures; the deviations are more pronounced for the shortest length scales, but still the fits yield very similar values for the critical temperature, which can be combined to

$$T_c(\rho = 1.042) = 0.445 \pm 0.010. \tag{8}$$

Within our error bars, this value coincides with the dynamical critical temperature obtained for the isobar $p = 1.0$. For the NVT-simulation the error bar is larger, since we were not able to equilibrate the melt as close to the dynamical critical temperature as was possible in the NpT-simulation. Note that the lowest temperature in figure 5(b) is $T = 0.46$, whereas it is $T = 0.5$ in figure 10. This difference is caused by the larger relaxation time in the NVT-ensemble (due to the higher density/pressure), at a specific temperature, in comparison to the

NpT-ensemble. Therefore the estimate becomes less accurate, but we can still conclude that the dynamical critical temperature of ideal MCT is indeed independent of the thermodynamic path chosen.

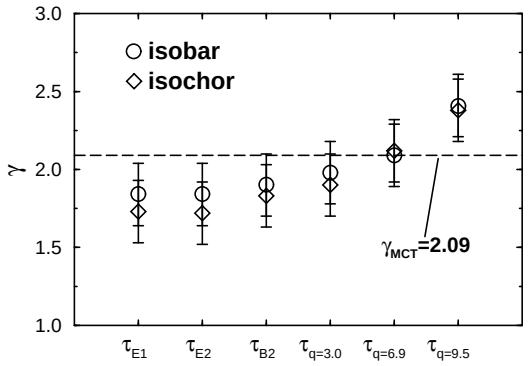

Figure 11. Values of γ determined from the temperature dependence of various correlation times, for two different thermodynamic paths, which yield the same critical temperature. On the abscissa, the relaxation times are quoted, from which γ was determined. For both the isobaric and the isochor path the error margins are about 10%, which is rather large, since γ is very sensitive to variation of the critical temperature. Within the error bars, γ does not depend on the thermodynamic path.

Finally, we want to verify that the exponent γ is independent of the thermodynamic path as well. As already discussed in section 3, the exponent γ shows a pronounced dependence on the dynamic correlation function considered, if one works with the same critical temperature for all quantities and extends the fit interval as much as possible. The same dependence is also found for the isochor, but the results coincide within the error bars with those of the isobars, as figure 11 illustrates. Therefore, γ is in fact independent of which path is chosen, which demonstrates the thermodynamic character of the dynamical critical point in mode-coupling theory.

5. Conclusions

In this paper we have presented results of a large-scale molecular dynamics simulation for a supercooled polymer melt. Our model is a coarse-grained bead–spring model with nonlinear springs connecting monomers along a chain and Lennard-Jones interactions between all monomers. By including competing length scales in the model we prevented the melt from crystallizing at lower temperatures.

The present study concentrated on the influence of pressure on the α-relaxation behaviour of the melt. Upon cooling we see a steep increase of the α-relaxation time, and all dynamic correlation functions show a two-step relaxation. By comparing data for different isobars, we found that our system exhibits not only time–temperature superposition above T_c, but time–temperature–pressure superposition as well.

For all pressures investigated, it has been possible to locate a temperature interval where the increase of the α-relaxation times could be described by idealized MCT. Therefore we have been able to investigate the dependence of the dynamical critical temperature of MCT on pressure and to give a sketch of the critical line in the (p, T) plane. However, whereas the critical temperatures determined from different quantities probing both small and large length

scales of the melt coincide within the error bars, the approach towards T_c, i.e., the exponent γ, is very sensitive to the precise choice of T_c in the fit, and depends on the quantity considered. When fixing T_c, we find that the α-relaxation times of $\phi_q^s(t)$ for q-values distributed around the maximum of the structure factor are compatible with the result of the β-analysis [39]. Deviations occur for much smaller and larger q-values. The deviations at large q can be explained by the sensitivity of γ to T_c, since fixing γ at the value of the β-analysis instead of T_c yields estimates for T_c that are compatible with the results of the β-analysis [39]. However, such an alternative fit procedure does not remove the discrepancies found on the largest length scale. On these length scales, γ is smaller than expected from the β-analysis. Similar deviations are also observed on smaller length scales, if the critical point is approached very closely. They can be rationalized, within the theoretical framework of MCT, by ergodicity-restoring processes which compete with and finally dominate over the cage effect treated by the idealized theory, if $T \leqslant T_c$. To what extent the predictions of the idealized theory are observable therefore depends not only on the quantity under consideration, which was also pointed out in recent theoretical work [16, 57], but also on the distance to the critical point. If one is too close, ergodicity-restoring processes interfere, and if the temperature is too large, the asymptotic regime, where the formulae of the idealized MCT are expected to hold, is departed from.

By performing simulations along an isochor which had the same intersection point with the critical line as one of the isobars, we have been able to verify that, within the error margin, the dynamical critical temperature of MCT is indeed independent of which thermodynamic path one chooses for the cooling. Furthermore, we have shown that the exponent γ does not depend on the choice of thermodynamic path either, within the caveats explained in the last paragraph.

In summary, one can therefore say that the idealized theory is a good starting point for a quantitative description of the dynamics above T_c, and seems to capture the essential physics, not only for simple liquids, but also for the polymer model. Why this could be the case is further discussed in reference [39].

Acknowledgments

We would like to thank W Kob, A Latz and B Dünweg for stimulating discussions, and also A Kopf for supplying his MD code. Support by the Sonderforschungsbereich SFB 262, and a generous grant of computer time from the computing centre at the University of Mainz and the HLRZ Jülich, are gratefully acknowledged.

References

[1] Jäckle J 1986 *Rep. Prog. Phys.* **49** 171
[2] Jäckle J 1987 *Phil. Mag.* B **56** 113
[3] Zallen R 1983 *The Physics of Amorphous Solids* (New York: Wiley)
[4] McKenna G B 1989 *Comprehensive Polymer Science* vol II, ed C Booth and C Price (New York: Pergamon) pp 311–62
[5] Götze W 1993 *Phase Transitions and Relaxations in Systems with Competing Energy Scales (NATO ASI Series C, vol 415)* ed T Riste and D Sherrington (Dordrecht: Kluwer)
[6] Cohen M H and Turnbull D 1959 *J. Chem. Phys.* **31** 1164
[7] Cohen M H and Turnbull D 1961 *J. Chem. Phys.* **34** 120
[8] Cohen M H and Turnbull D 1970 *J. Chem. Phys.* **52** 3038
[9] Gibbs J H and Di Marzio E A 1958 *J. Chem. Phys.* **28** 373
[10] Gibbs J H and Di Marzio E A 1958 *J. Chem. Phys.* **28** 807
[11] Adam G and Gibbs J H 1965 *J. Chem. Phys.* **43** 139
[12] Di Marzio E A and Young A J M 1997 *J. Res. NIST* **102** 135

[13] Li G, Du W M, Chen X K, Tao N J and Cummins H Z 1992 *Phys. Rev.* A **45** 3867
Cummins H Z, Du W M, Fuchs M, Götze W, Hildebrand S, Latz A, Li G and Tao N J 1993 *Phys. Rev.* E **47** 4223
[14] van Megen W and Underwood S M 1993 *Phys. Rev.* E **47** 248
van Megen W and Underwood S M 1994 *Phys. Rev.* E **49** 4206
van Megen W, Mortensen T C, Williams S R and Müller J 1998 *Phys. Rev.* E **58** 6073
[15] Cummins H Z, Li G, Du W M and Hernandez J 1994 *Physica* A **204** 169
[16] Franosch T, Götze W, Mayr M R and Singh A P 1997 *Phys. Rev.* E **55** 3183
[17] Tölle A, Schober H, Wuttke J and Fujara F 1997 *Phys. Rev.* E **56** 809
[18] Baschnagel J 1994 *Phys. Rev.* B **49** 135
[19] Baschnagel J and Fuchs M 1995 *J. Phys.: Condens. Matter* **7** 6761
[20] Kob W and Andersen H C 1995 *Phys. Rev.* E **51** 4626
[21] Kob W and Andersen H C 1995 *Phys. Rev.* E **52** 4134
[22] Kämmerer S, Kob W and Schilling R 1997 *Phys. Rev.* E **56** 5450
[23] Kämmerer S, Kob W and Schilling R 1998 *Phys. Rev.* E **58** 2131
[24] Kämmerer S, Kob W and Schilling R 1998 *Phys. Rev.* E **58** 2141
[25] Sciortino F, Fabbian L, Chen S-H and Tartaglia P 1997 *Phys. Rev.* E **56** 5397
[26] Bennemann C, Paul W, Binder K and Dünweg B 1998 *Phys. Rev.* E **57** 843
[27] Yip S and Nelson P (ed) 1995 *Transport Theory Stat. Phys.* **24** Nos 6–8 (Theme Issues on mode-coupling theory)
[28] Bengtzelius U, Götze W and Sjölander A 1984 *J. Phys. C: Solid State Phys.* **17** 5915
[29] Götze W 1990 *Liquids, Freezing and Glass Transition* part 1, ed J-P Hansen, D Levesque and J Zinn-Justin (Amsterdam: North-Holland) pp 287–503
[30] Götze W and Sjögren L 1992 *Rep. Prog. Phys.* **55** 241
[31] Götze W and Sjögren L 1995 *Transport Theory Stat. Phys.* **24** 801
[32] Schilling R 1994 *Disorder Effects on Relaxational Processes* ed R Richert and A Blumen (Berlin: Springer)
[33] Kob W 1997 *Experimental and Theoretical Approaches to Supercooled Liquids: Advances and Novel Application* ed J T Fourkas, D Kivelson, U Mohanty and K A Nelson (Washington, DC: ACS Books)
[34] Bengtzelius U 1986 *Phys. Rev.* A **33** 3433
[35] Li G, King H E, Oliver W F, Herbst C A and Cummins H Z 1995 *Phys. Rev. Lett.* **74** 2280
[36] Tölle A 1997 *Doctoral Thesis* Dortmund University
[37] Tölle A, Schober H, Wuttke J, Randl O G and Fujara F 1998 *Phys. Rev. Lett.* **80** 2374
[38] Angell C A and Sichina W 1976 *Ann. NY Acad. Sci.* **279** 53
[39] Bennemann C, Baschnagel J and Paul W 1999 *Eur. Phys. J.* B submitted
(Bennemann C, Baschnagel J and Paul W 1998 Molecular dynamics simulation of a glassy polymer melt: incoherent scattering function *Preprint* cond-mat/9809335)
[40] Kremer K and Grest G S 1990 *J. Chem. Phys.* **92** 5057
[41] Dünweg B, Grest G S and Kremer K 1997 *Conf. Proc. of the IMA Workshop (Minneapolis, MN, May 1996)* (Berlin: Springer)
[42] Kopf A, Dünweg B and Paul W 1997 *J. Chem. Phys.* **107** 6945
[43] Wolfgardt M, Baschnagel J, Paul W and Binder K 1996 *Phys. Rev.* E **54** 1535
[44] Wolfgardt M and Binder K 1996 *Macromol. Theory Simul.* **5** 699
[45] Nosé S 1991 *Prog. Theor. Phys. Suppl.* **103** 1
[46] Hoover W G 1985 *Phys. Rev.* A **31** 1695
[47] Di Tolla D and Ronchetti M 1993 *Phys. Rev.* E **48** 1726
[48] Bennemann C 1998 *Doctoral Thesis* Mainz University
[49] Schilling R and Scheidsteger T 1997 *Phys. Rev.* E **56** 2932
[50] Scheidsteger T and Schilling R 1998 *Phil. Mag.* B **77** 3
[51] Bernu B, Hansen J-P, Hiwatari Y and Pastore G 1989 *Phys. Rev.* A **51** 4891
[52] Roux J N, Barrat J L and Hansen J-P 1989 *J. Phys.: Condens. Matter* **1** 7171
[53] Barrat J L and Latz A 1990 *J. Phys.: Condens. Matter* **2** 4289
[54] Nauroth M and Kob W 1997 *Phys. Rev.* E **55** 657
[55] Lunkenheimer P, Pimenov A, Dressel M, Schiener B, Schneider U and Loidl A 1997 *Prog. Theor. Phys. Suppl.* **126** 123
[56] Bennemann C, Paul W, Baschnagel J and Binder K 1999 Molecular dynamics simulation of a glassy polymer melt: Rouse modes and mean square displacements *Comput. Theor. Polym. Sci.* at press
[57] Fuchs M, Götze W and Mayr M R 1998 *Phys. Rev.* E **58** 3389